npj | Quantum Materials

www.nature.com/npjquantmats

REVIEW ARTICLE OPEN

Milestones of low-D quantum magnetism

Alexander Vasiliev[1,2,3], Olga Volkova[1,2,3], Elena Zvereva[1,2] and Maria Markina[1]

There is a long time gap between the formulation of the basic theory of low-dimensional (low-D) magnetism as advanced by Ising, Heisenberg and Bethe and its experimental verification. The latter started not long before the discovery of high-T_C superconductivity in cuprates and has been boosted by this discovery result in an impressive succession of newly observed physical phenomena. Milestones on this road were the compounds which reached their quantum ground states upon lowering the temperature either gradually or through different instabilities. The gapless and gapped ground states for spin excitations in these compounds are inherent for isolated half-integer spin and integer spin chains, respectively. The same is true for the compounds hosting odd and even leg spin ladders. Some complex oxides of transition metals reach gapped ground state by means of spin-Peierls transition, charge ordering or orbital ordering mechanisms. However, the overwhelming majority of low-dimensional systems arrive to a long-range ordered magnetic state, albeit quite exotic realizations. Under a magnetic field some frustrated magnets stabilize multipolar order, e.g., showing a spin-nematic state in the simplest quadropolar case. Finally, numerous square, triangular, kagome and honeycomb layered lattices, along with Shastry–Sutherland and Nersesyan–Tsvelik patterns constitute the playground to check the basic concepts of two-dimensional magnetism, including resonating valence bond state, Berezinskii–Kosterlitz–Thouless transition and Kitaev model.

npj Quantum Materials (2018)3:18 ; doi:10.1038/s41535-018-0090-7

INTRODUCTION

Milestones in the field of low-dimensional magnetism, similar to posts along the road, lead to a very attractive destination, i.e., the formulation of a coherent and unified picture of quantum cooperative phenomena in solids. The story begins in 1925 when Ising following the advice of his tutor Lenz considered infinite chain of magnetic moments with nearest neighbor interaction only.[1] The Hamiltonian considered in this case is valid for the preferred component of the spin ***S***

$$H_{Ising} = J\sum_n (S_n^z S_{n+1}^z) \quad (1)$$

No spontaneous magnetization at any finite temperature was found within frames of this model. Opposite is the isotropic Heisenberg case[2]

$$H_{\text{Heisenberg}} = J\sum_n (S_n^x S_{n+1}^x + S_n^y S_{n+1}^y + S_n^z S_{n+1}^z) \quad (2)$$

The ground states of uniform $S = 1/2$ chains are different in these two models. While the chain becomes ordered at zero-temperature in the Ising limit, it remains disordered even at zero-temperature in the Heisenberg limit. In 1931, Bethe introduced his famous "ansatz" method to find the exact quantum ground state of the antiferromagnetic Heisenberg model in one dimension.[3] The extension of classical Ising model to two dimensions was provided by Onsager in 1944.[4] Such a system orders magnetically at finite temperature comparable to the value of exchange interaction parameter J. Two-dimensional Heisenberg system remains disordered at finite temperatures, but its ground state is ordered. The basic role in low dimensional magnetism belongs to Mermin-Wagner theorem formulated in 1966.[5] It states that no one-dimensional or two-dimensional isotropic Heisenberg spin system can order either ferromagnetically or antiferromagnetically at any non-zero temperature.

In the case when the moments lie perpendicular to the chosen axis the model Hamiltonian is

$$H_{XY} = J\sum_n (S_n^x S_{n+1}^x + S_n^y S_{n+1}^y) \quad (3)$$

Two dimensional antiferromagnets of XY type form magnetic vortices and antivortices within the plane. The diameters of these objects grow upon cooling. The vortices contact each other at Berezinskii–Kosterlitz–Thouless (BKT) temperature resulting in a unique form of long-range order without spontaneous magnetization.[6–8] An important difference between integer and half-integer spin chains was admitted by Haldane in 1983.[9] The uniform spin-1/2 chain is gapless, it has fractionalized excitations—domain walls carrying spin $S = 1/2$. These excitations are confined when chains are coupled into ladders or when there is an alternation of exchange interaction. The uniform spin-1 chain is gapped and the excitations are triplets.

Overall, the properties of magnetic systems depend on their symmetry and dimensionality D. Discrete symmetry (Ising model) can be broken at $T = 0$ in $D = 1$ and cannot be broken at finite T. Continuous Abelian symmetry (XY model) cannot be broken in $D = 1$, but at $T = 0$ the correlations decay as power law. In $D = 2$ correlations decay as power law at finite T and become exponential above BKT transition. Continuous non-Abelian symmetry SU(2) (Heisenberg model) cannot be broken in $D = 1$ even at $T = 0$ and can be broken spontaneously only at $T = 0$ in D = 2.

[1]Lomonosov Moscow State University Moscow 119991, Russia ; [2]National Research South Ural State University Chelyabinsk 454080, Russia and [3]National University of Science and Technology "MISiS" Moscow 119049, Russia
Correspondence: Alexander Vasiliev (vasil@mig.phys.msu.ru)

Received: 29 September 2017 Revised: 14 February 2018 Accepted: 26 February 2018
Published online: 28 March 2018

The exotic phenomena mentioned in this review are realized in quantum magnets being localized low-spin systems, either spin-1/2 or spin-1, not large classical moments. An attractive feature of some low-dimensional magnets is a spin-liquid state defying a long-range order. The liquid may be either gapped or gapless, dependent on the type of quantum statistics. Adjacent to low-dimensionality is the field of spin frustration, these two phenomena being frequently coexisting in real magnets. The spin-liquid ground state may survive in the presence of strong interaction between magnetic entities, albeit long-range magnetic order establishes itself most frequently in solids upon lowering the temperature due to residual interactions in three dimensions. Numerous attempts were undertaken to find higher-dimensional analogs of the one-dimensional spin−1/2 Heisenberg antiferromagnet (AFM) in a state that breaks neither translational nor spin rotational symmetry. Apart from the isolated ions, the dimers, i.e., two spins coupled by positive (antiferromagnetic) exchange interaction J, seem to be the simplest objects of low-dimensional magnetism. The singlet rotationally invariant ground state of isolated dimers is separated in energy from the triplet excited state by the excitation gap $\Delta = J$. The interaction between moments belonging to different dimers, may it be of spin or spin-lattice type, leads to remarkable cooperative phenomena.

The outline of the review is as follows. The 0D objects of quantum low-dimensional magnetism, i.e., spin-1/2 dimers, exhibit a cooperative behavior when coupled. Multiple plateaus appear in magnetization of Shastry–Sutherland dimers network due to the formation of regular patterns of triplet excitations. The plateaus in magnetization can be considered as intermediate Mott insulator phases separating the domes of Bose–Einstein condensation of magnons. Giamarchi, Ruegg and Tchernyshyov underpin the basic concepts of this phenomenon including a detailed correspondence between a Bose gas and a quantum antiferromagnet.[10] Bose–Einstein condensation of magnons is not restricted to spin-1/2 dimers, the representative examples are spin-1 dimers and spin-1 ions with strong anisotropy also.

The chains, either gapped or gapless, represent an evident move from 0D to 1D. The description of uniform and alternating half-integer spin chains is complimented by short detour to integer spin chains. Various phase transitions may bring uniform spin-1/2 chain into ground state with a gap in magnetic excitation spectrum. Among them, spin-Peierls transition, charge ordering and orbital ordering effects can be distinguished. The routine scenario for quasi-one-dimensional system is an eventual 3D order, albeit quite exotic sometimes. Numerous features of this order—chirality, incommensurability, nematicity—make this field of study attractive.

Spin-ladders, to be considered intermediate between 1D and 2D systems, may show either gapped or gapless behavior dependent on leg number. The ladder system can be extended to Nersesyan–Tsvelik network, whose properties are described in some details. As the dimensionality of the system increases, the richer becomes the spectrum of observed magnetic phenomena. It is out of question to list all of them in a short review, but some issues related to 2D square, triangular, kagome and honeycomb lattices are mentioned. The conclusion is supplemented by list of selected spin gap compounds of authors' choice.

DIMERS, SHASTRY–SUTHERLAND NETWORK

A set of orthogonal dimers coupled by frustrated interdimer interaction constitutes the network described by the Shastry–Sutherland model[11,12]

$$H = J\sum_{nn} S_i \cdot S_j + J'\sum_{nnn} S_i \cdot S_j \quad (4)$$

It is assumed that both intradimer J and interdimer J' exchange interactions are positive. Dependent on $\alpha = J'/J$ ratio, the ground state of this model is either spin singlet ($\alpha < \alpha_C$) or Neel order ($\alpha > \alpha_C$), where α_C ~0.7.

A good realization of the Shastry–Sutherland model is the $SrCu_2(BO_3)_2$.[13] The temperature dependence of the magnetic susceptibility χ in $SrCu_2(BO_3)_2$ is shown in Fig. 1a. At around $T =$ 20 K, a steep drop evidences the presence of a spin gap and the singlet/non-magnetic ground state. Evidently, neither the isolated spin dimer model (solid line) nor its mean field modification (dashed line) describes the experimental data. The numerical analysis[12] has shown that the peculiar shape of the $\chi(T)$ curve is due to the fact that the ratio of $J = 100$ K and $J' = 68$ K in $SrCu_2(BO_3)_2$ is quite close to the transition point α_C. The almost dispersionless spin gap $\Delta = 34$ K was evaluated in inelastic neutron scattering.[14]

Another attractive feature of $SrCu_2(BO_3)_2$ is the sequence of plateaus in magnetization, as shown in the inset to Fig. 1a. Plateaus are due to the strong localization of the triplet excitations within the set of orthogonal dimers. At the fractions of magnetization, where the triplets create a superstructure, the energy is at a local minimum. At present, the magnetization in $SrCu_2(BO_3)_2$ investigated in static magnetic fields up to 34 T has revealed the plateaus at 1/8, 2/15, 1/6 and 1/4 of the saturation,[15]

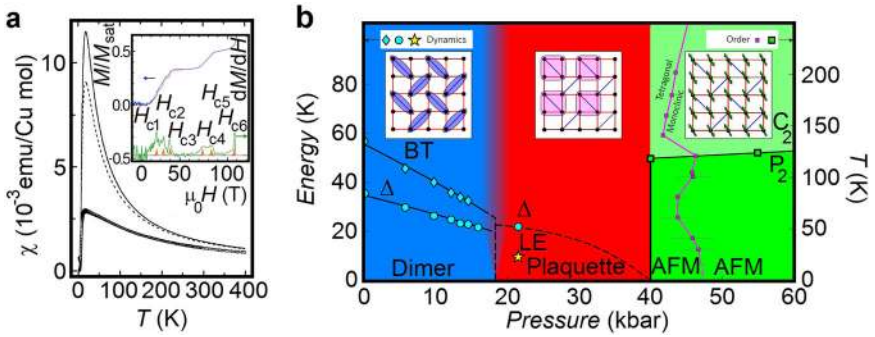

Fig. 1 **a** Temperature dependence of magnetic susceptibility $\chi = M/H$ in $SrCu_2(BO_3)_2$ taken at $\mu_0 H = 1$ T (adapted with permission from, ref. 13 copyright American Physical Society 1999). The solid and dashed lines are fitting curves. Inset represents the field dependencies of reduced magnetization M/M_{sat} and its derivative dM/dH taken at $T = 2.1$ K for $H//c$ axis (adapted with permission from, ref. 16 copyright American Physical Society 2013). The critical fields H_i associated with the plateaus are marked by vertical arrows; **b** Phase diagram of $SrCu_2(BO_3)_2$ (adapted with permission from, ref. 19 copyright Springer Nature 2017). Green circles correspond to the triplet gap Δ at $Q = (2,0,L)$, two-triplet bound state (BT) is marked by green diamonds; the dashed line is the extrapolated energy gap and yellow star denotes a new low-energy excitation (LE) at $Q = (1,0,1)$. Green squares denote magnetic Bragg peaks at $Q = (1,0,0)$. Magenta line marks the structural transition. Insets represent dimer, plaquette and Neel ground states

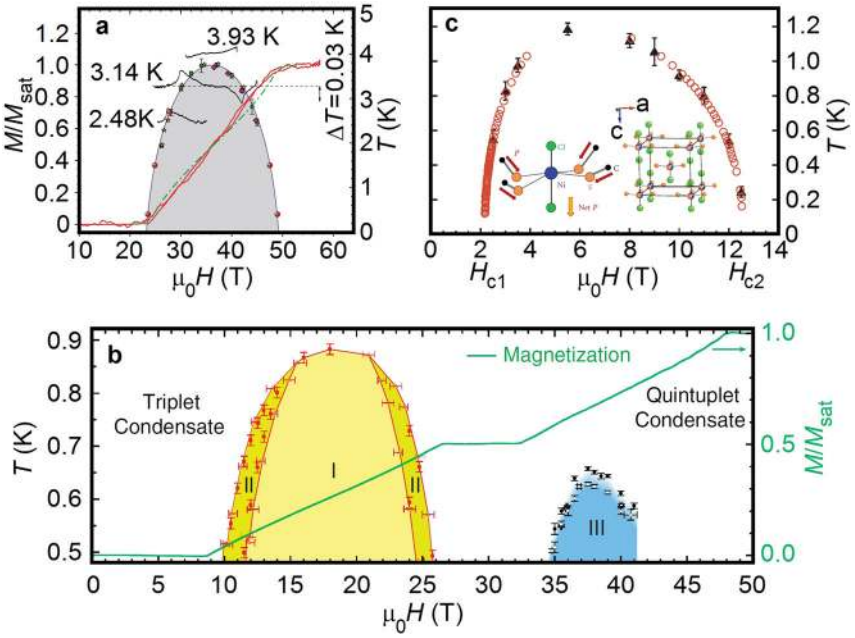

Fig. 2 The phase diagrams of BEC. Symbols represent the data of specific heat and magnetocaloric (MC) measurements. **a** $BaCuSi_2O_6$, experimental (solid) and calculated (dash) magnetization curves at 1.5 K for *H*//*c* axis (lines), ΔT refers to MC effect (adapted with permission from, ref. 23 copyright American Physical Society 2009); **b** $Ba_3Mn_2O_8$, the phases I and III are marked as measured for *H*//*c* axis, phase II appears at *H*//*a* axis (reproduced with permission from, ref. 25 copyright American Physical Society 2009); **c** $NiCl_2$-4SC$(NH_2)_2$, the inset depicts the crystal structure (adapted with permission from, ref. 27 copyright American Physical Society 2006)

while the measurements in pulsed magnetic fields identified additionally 1/3 and 1/2 plateaus.[16] The plateau regions correspond to the spin-gapped states with the stripe order of triplets. It has been argued that the sequence of field-induced phases observed in $SrCu_2(BO_3)_2$ represents the first example of an incomplete devil's staircase concerning magnetization of the quantum AFM[15] where the lower plateaus should be described by a superlattice of triplets of the four-Cu spins, instead of dimer triplets.[17]

The plaquette phase intermediate between the dimerized spin-singlet state ($\alpha = 0$) and Neel order ($\alpha \to \infty$) has been predicted in zero magnetic field for the Shastry–Sutherland network at $0.68 < \alpha < 0.86$.[18] This phase has been identified recently in inelastic neutron scattering performed on $SrCu_2(BO_3)_2$ single crystal under pressure up to 60 kbar.[19] As shown in Fig. 1b (left panel), the dimer phase exists up to $P = 16$ kbar, where both the gap and the energy of bound triplets decrease. In the range $P = 21.5 \div 40$ kbar, the new plaquette phase with a spin gap $\Delta \sim 23$ K is identified, as shown in Fig. 1b (middle panel). Eventually, the gap closes under pressure and Neel ordering takes place at $P = 40$ kbar. The transition between dimer and plaquette phases is of the first order in the range $P = 16 \div 21.5$ kbar, while the transition between the plaquette singlet and Neel phase is of the second order. As shown in Fig. 1b (right panel), a further increase in pressure results in a tetragonal monoclinic structural phase transition, where the Cu^{2+} spin dimers are no more orthogonal.

DIMERS, BOSE–EINSTEIN CONDENSATION

The ground state energy of a system consisting of integer spin particles, bosons, can be minimized via spontaneous Bose–Einstein condensation (BEC), without any interaction. This phenomenon predicted initially for the photons is considered responsible for superfluidity and superconductivity, refer to condensation of trapped atomic gases and can also be applied to quasiparticles in a solid.[20] Note that the concept of BEC with regard to the spin systems is only an approximation: exchange anisotropy and single-ion anisotropy always break rotational symmetry. Magnons are bosons irrespective of the ions magnetic moment. At low temperatures, the BEC was observed in Heisenberg or axially symmetric low-dimensional magnets with spin-singlet ground state, e.g., spin-1/2 dimers[21–25] and composite integer spin chains[26] or in the systems with strong single-ion anisotropy.[27] The BEC occurs under action of magnetic field which splits the triplet $S = 1$ and lowers the energy of $S_z = 1$ level. At the first critical field H_{C1}, the $S = 0$ and $S_z = 1$ levels cross starting the process of BEC. At low temperatures, the formation of new state is manifested by sharp anomalies in magnetization and specific heat, whose magnitude increases with magnetic field. In the range $H_{C1} < H < H_{C2}$, the canted AFM state exists with net magnetization proportional to the magnetic field. At the second critical field H_{C2}, the magnetization saturates. In the vicinity of H_{C1}, the phase boundary for a three-dimensional system should follow the power law $H_{C1}(T) - H_{C1}(0) \sim T^{3/2}$.

At present, BEC phenomena have been reported at finite temperatures for a number of quantum magnets.[28] Three representative cases are the systems of spin-1/2 dimers, spin-1 dimers and isolated $S = 1$ ions. The ancient Han purple pigment, $BaCuSi_2O_6$, is a spin gap compound with a square lattice of dimers forming the bilayer structure.[23] Along the *c* axis, the Cu^{2+} ions, $S = 1/2$, are coupled by $J = \Delta = 52$ K. In addition, these ions are coupled in the *ab* plane by $J' = 7$ K. The BEC critical fields in $BaCuSi_2O_6$ are $\mu_0 H_{C1} = 23.5$ T and $\mu_0 H_{C2} = 49$ T with $T_{max} = 3.8$ K. The dome shaped phase boundary of the ordered phase in $BaCuSi_2O_6$ is shown in Fig. 2a. This boundary is marked by sharp anomalies in specific heat and magnetocaloric effect.

The singlet−triplet and triplet−quintuplet BEC was studied in the spin-1 dimer compound, $Ba_3Mn_2O_8$.[25] Its magnetic subsystem is comprised of pairs of Mn^{5+} ions arranged on triangular lattice and coupled along the *c* axis by $J = 19$ K. The multiple interactions between dimers amount to $J' \sim 1$ K, while the single-ion uniaxial anisotropy is $D \sim 0.3$ K. The ground state of $S = 1$ dimers is the singlet; the first excited state is the triplet $S = 1$ ($\Delta_1 = J$); and the second one is the quintuplet $S = 2$ ($\Delta_2 = 3J$). Under magnetic field

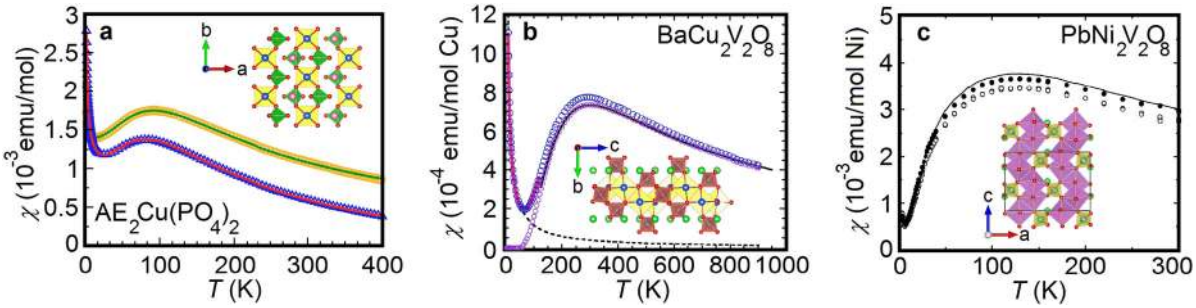

Fig. 3 Temperature dependencies of magnetic susceptibility χ in spin chain systems. **a** gapless uniform spin-1/2 chains in $Sr_2Cu(PO_4)_2$ and $Ba_2CuP_2O_8$(adapted with permission from, ref. 33 copyright American Physical Society 2006); **b** gapped alternating spin-1/2 chain in $BaCu_2V_2O_8$ (adapted with permission from, ref. 39 copyright American Physical Society 2004), the dotted line is an extrapolation of impurities term; **c** gapped uniform spin-1 chain in $PbNi_2V_2O_8$ (adapted with permission from, ref. 47 copyright American Physical Society 1999). The fragments of crystal structures are depicted in the insets in each panel

both excited states split and levels $S_z = 1$ and later $S_z = 2$ cross the ground state level. The field dependence of magnetization of $Ba_3Mn_2O_8$ demonstrates two linear regions corresponding to BEC, as shown in Fig. 2b. At $T = 0.5$ K, the critical fields for triplet BEC are $\mu_0 H_{C1} = 8.73$ T and $\mu_0 H_{C2} = 26.46$ T with $T_{max1} = 0.86$ K, while for the quintuplet BEC $\mu_0 H_{C3} = 32{,}42$ T and $\mu_0 H_{C4} = 47.9$ T with $T_{max2} = 0.63$ K. The magnetization plateau in the range $\mu_0 H_{C2}$–$\mu_0 H_{C3}$ corresponds to one S = 1 triplet per dimer. Two dome-shaped phase diagram in $Ba_3Mn_2O_8$ for field perpendicular to the *c* axis is shown in Fig. 2b. The regions I and II correspond to different phases of the triplet condensate; the region III corresponds to the quintuplet condensate.[29]

A qualitatively different case of BEC is represented by $NiCl_2$-4SC $(NH_2)_2$ (DTN), where the gap between singlet $S = 0$ and doublet $S_z = \pm 1$ levels is due to a single-ion anisotropy $D = \Delta = 8$ K of isolated $S = 1$ Ni^{2+} ions.[27] In this compound, the nickel ions are surrounded by four polar molecules of thiourea, making the DTN a molecular magnet. Similar to dimers, an external magnetic field shifts down the $S_z = 1$ level. The critical fields in DTN are $\mu_0 H_{C1} = 2$ T and $\mu_0 H_{C2} = 12.5$ T with $T_{max} = 1.2$ K (Fig. 2c). In variance with the dimer systems where the gap is basically isotropic, the properties of DTN strongly depend upon the direction of the magnetic field with respect to the easy magnetization axis.

CHAINS, SPIN LIQUIDS

The uniform half-integer spin chain does not present a gap in the triplet excitation spectrum. The chain is disordered in an isotropic case but the anisotropy of exchange interaction results in a long-range order at $T = 0$ K.[30] The system with small exchange anisotropy can be described by the pure Heisenberg form JS_iS_j while the Ising form $JS_i^zS_j^z$ should be applied to the highly anisotropic case.[31] The $\chi(T)$ curve of Heisenberg AFM spin-1/2 chain demonstrates a broad maximum at T_{max} ~0.64 *J*. Below this temperature, it is reduced by ~15%. At the same time, the Ising chain demonstrates a broad maximum in $\chi(T)$ curve at $T_{max} = 0.5\,J$ and its reduction to zero at $T = 0$ K. There are many good examples of uniform Heisenberg spin-1/2 chains, among them $AE_2Cu(PO_4)_2$ (AE = Sr, Ba).[32] The broad maxima in $\chi(T)$ curves are seen at $T_{max} = 92$ K ($J = 143$ K) for the Sr- and $T_{max} = 82$ K ($J = 132$ K) for the Ba-compounds (Fig. 3a). Although the $Sr_2Cu(PO_4)_2$ seems to be the best realization of a Heisenberg spin-1/2 chain,[33] the measurements of *ac*–susceptibility identified the long-range order in the Sr-compound at $T_N = 0.085$ K.[34]

An alternation of the exchange interaction along the spin-1/2 chain, J_1–J_2, leads to the appearance of a spin gap in the excitation spectrum. The confined excitations carry spin 0 and 1, the gap for triplet excitations is located at $q = \pi$.[35] Depending on the alternation parameter $0 \le a = J_2/J_1 \le 1$ two limiting cases can be considered. For $a = 0$, the chain transforms into a set of isolated dimers; for $a = 1$, it is the uniform chain. In the range $0 \le a \le 0.9$, the spin gap is defined as $\Delta = J_1(1-a)^{3/4}(1+a)^{1/4}$.[36] In the case of ferromagnetic (FM) exchange interaction J_2 alternating with AFM J_1, the energy spectrum is gapped also. The gap is located at $q = \pi/2$ similar to the AFM Heisenberg $S = 1$ chain.[37] The $\chi(T)$ curves show the correlation maximum, which shifts from T_{max} ~$0.64J_1$ at $a = |J_2|/J_1 = 0$ to lower temperatures with a increasing.[38] An alternating spin-1/2 chain compound with a large spin gap is $BaCu_2V_2O_8$.[39] The $\chi(T)$ curve demonstrates a broad maximum at $T_{max} \approx 280$ K (Fig. 3b) which enables estimation of a leading exchange interaction as $J_1 = 460$ K. The spin gap found in ^{51}V NMR measurements amounts to 380 K.[40] While first principles calculations identified $BaCu_2V_2O_8$ as an AFM–AFM chain compound with a equal to either 0.16 (Ref. [41]) or 0.05 (Ref. [42]), recent high-resolution inelastic neutron scattering data unveiled an AFM–FM alternating chain with $J_1 = 475$ K and $J_2 = -140$ K.[43]

Integer spin chains with sufficiently weak anisotropy are characterized by a nonmagnetic singlet ground state and a nonzero excitation-energy gap.[44] Hamiltonian of spin-1 chain is

$$H = |J| \sum_n \left[\vec{S}_n \cdot \vec{S}_{n+1} + \lambda S_n^z S_{n+1}^z + \mu \left(S_n^z\right)^2 \right], \quad (5)$$

where λ is the exchange interaction anisotropy and μ is the crystal field splitting of the single ion levels. The gapped phase exists in an extended range of exchange anisotropy $0 \le \lambda \le 1.18$ for $\mu = 0$.[45] Moreover, for $\lambda \approx 1$, the gap decreases, goes through a minimum, estimated to be zero, and then increases with positive μ. Monte Carlo calculations performed for spin-1 AFM Heisenberg chain estimate the gap $\Delta = 0.41\,J$.[46] $PbNi_2V_2O_8$ is considered to be an example of the Haldane chain conjecture. The $\chi(T)$ curve evidences the presence of the gap in the energy spectrum (Fig. 3c). The position of the broad maximum at $T_{max} = 120$ K allows estimating $J = 95$ K and $\Delta = 39$ K.[47] However, the determination of the spin gap from magnetization curves gives a lower value $\Delta = (2\Delta_\perp + \Delta_\parallel)/3 = 22$ K. This is ascribed to the presence of both interchain interactions $J_\perp$ and negative single ion anisotropy D. In inelastic neutron scattering the main magnetic parameters in $PbNi_2V_2O_8$ were estimated as $J = 110$ K, $J_\perp = 1$ K and $D = -2.7$ K. The values of transverse and longitudinal gaps constituted $\Delta_\perp = 48$ K and $\Delta_\parallel = 43$ K.[48] The D/J and $J_\perp/J$ ratios put $Pb_2Ni_2V_2O_8$ system in the Haldane phase near the border with the ordered Ising-like phase in the D-$J_\perp$ phase diagram.[46]

CHAINS, PHASE TRANSITIONS, SPIN GAP

The uniform spin-1/2 chains are unstable with respect to various effects leading to a spin gap formation. The interactions of spin, charge and orbital degrees of freedom with the lattice lead to the spin-Peierls transition, charge and orbital order driven transitions.

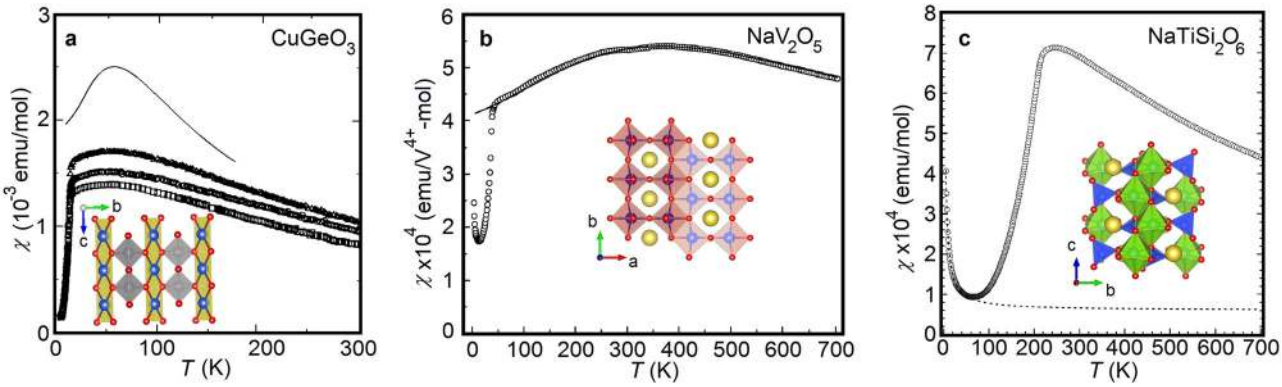

Fig. 4 **a** The spin-Peierls transition in $CuGeO_3$ (adapted with permission from, ref. 50 copyright American Physical Society 1993). Symbols represent the experimental data taken along three principal axes; **b** The charge ordering transition in NaV_2O_5 (adapted with permission from, ref. 56 copyright Physical Society of Japan 1996). **c** The orbital ordering transition in $NaTiSi_2O_6$ (adapted with permission from, ref. 61 copyright Physical Society of Japan 2002). The solid lines in **b** and **c** represent the Bonner–Fisher curve. The dashed line in panel *c* represents the Curie–Weiss law. All measurements were taken at $\mu_0 H = 1$ T. The fragments of crystal structures are depicted in the insets in each panel

All of them include structural distortion and in every case a loss in elastic energy is compensated by a gain in magnetic energy.

The spin-Peierls transition, being the most unusual kind of magnetoelastic transition, relates to the particular quantum mechanical nature of quasi-one-dimensional AFM. Similar to the Peierls transition in quasi-one-dimensional conductors, the spin-Peierls transition integrates spin gap formation and dimerization of the underlying crystal lattice. This phenomenon, found initially in tetrathiafulvalene-$CuS_4C_4(CF_3)_4$ at $T_{SP} = 12$ K,[49] was observed later in $CuGeO_3$.[50] In contrast to the AFM transition, the reduction of magnetic susceptibility χ at the spin-Peierls transition is isotropic. This is illustrated by χ(*T*) curves measured along three principal axes in $CuGeO_3$ (Fig. 4a). The broad correlation maximum is reached at $T_{max} = 56$ K, which defines the intrachain exchange interaction along the *c* axis $J = 88$ K. The spin-Peierls transition is manifested by a sharp drop in the χ(*T*) curve at $T_{SP} = 14$ K. Under magnetic field, the transition shifts to lower temperatures $\sim aH^2$ with $a = 0.46$.[51] At $T < T_{SP}$, two alternating *J*'s form, i.e., $J_{1,2}(T) = J(1 \pm \delta(T))$. The spin gap $\Delta = 24$ K is proportional to the alternation $\delta = 0.17$. The values of interchain exchange interactions along the *b* axis $J_b = 0.1\,J$ and *c* axis $J_c = -0.01\,J$ were provided by inelastic neutron scattering.[52] All spin-Peierls compounds obey universal magnetic phase diagram comprised of uniform, dimerized and intermediate phases.[53] The last one is considered to be a commensurate, discommensurate (a magnetic soliton), or incommensurate phase. The critical field of the transition between dimerized and intermediate phases in $CuGeO_3$ is 12-13 T.[54] Full saturation of magnetization in $CuGeO_3$ was achieved at $\mu_0 H = 253$ T in pulsed magnetic field measurements.[55]

A charge-ordering-driven phase transition into the spin gap state was observed in the NaV_2O_5 at $T_C = 35$ K (Fig. 4b).[56] At elevated temperatures, the average oxidation state of vanadium ions is $V^{4.5+}$. Below T_C, two distinctly different oxidation states were evidenced in V^{51} NMR measurements which also identified a spin gap value $\Delta = 108$ K.[57] At low temperatures, the monoclinic *A*112 structure of NaV_2O_5 is constituted by enlarged unit cell $(a\text{-}b) \times 2b \times 4c$, where *a*, *b* and *c* are the crystal lattice parameters of the high-temperature orthorhombic phase.[58] At $T \le T_C$, the temperature-dependent charge disproportionation $V^{4.5\pm\delta c/2}$ was observed with continuous variation of δ_c.[59] The fully charged zigzag-type pattern differs distinctly from the chain-type considered a prerequisite to the spin-Peierls state. At present, the alternation of exchange interaction within zigzag chain is considered to be responsible for a spin gap. The low temperature crystal structure in NaV_2O_5 is fixed by both lattice distortion and Coulomb repulsion. These two factors are responsible also for the "devil's staircase" phase transitions between commensurate phases with $2a \times 2b \times zc$ type superstructures found in NaV_2O_5.[60]

A spin-Peierls-like phase transition[61] driven by spin-orbital fluctuations[62] was observed in $NaTiSi_2O_6$. The transition takes place at $T_C = 210$ K which is higher than the temperature of correlation maximum in χ(*T*) curve.[31] In this case, the short-range order within the chains is not fully developed and solely magnetic fluctuations cannot be considered to be the driving force. $NaTiSi_2O_6$ hosts the skew-edge-sharing chain of slightly distorted TiO_6 octahedra in monoclinic *C*2/*c* structure.[63] At elevated temperatures, the fluctuations of the orbital degrees of freedom allow $NaTiSi_2O_6$ to be considered as a dynamic Jahn−Teller phase.[64] At $T_C = 210$ K, $NaTiSi_2O_6$ transforms to triclinic $P\bar{1}$modification[63] which is accompanied by a gradual decrease in magnetic susceptibility (Fig. 4c). The exchange interaction *J* along the chain is provided by the overlap of nearly degenerated $|xy\rangle$ and $|yz\rangle$ orbitals ($|xz\rangle$ orbitals are non-bonding). Taking into consideration the orbital degree of freedom, the Hamiltonian of this system can be written as[64]

$$H = |J| \sum_{i,j} S_i \cdot S_j \left[\frac{1}{4} + T_i^z T_j^z + \frac{(-1)^i}{2} (T_i^z + T_j^z) \right], \tag{6}$$

where the orbital operator $T_i^z = 1/2$ corresponds to an occupied $|xy\rangle$ orbital and $T_i^z = -1/2$ to an occupied $|yz\rangle$ orbital. The ground state of this Hamitonian is a dimerized orbital-ordered one hosting the spin singlet on each bond. The states with either $|xy\rangle$ or $|yz\rangle$ occupied are degenerated. The condensation of the system in either one of these states explains the appearance of a large singlet-triplet spin gap. The value of gap $\Delta = 620$ K was estimated in time-of-flight neutron spectroscopy[65] in good correspondence with the first principles calculations.[66]

CHAINS, PHASE TRANSITIONS, LONG-RANGE ORDER

The long-range order is the final destination for numerous quasi-one-dimensional magnets not protected by a spin gap. This is because the weak interchain exchange interactions *J'* inevitably come into play upon lowering the temperature. The ground state of these systems also depends on both signs and values of nearest neighbor J_{nn} and next nearest neighbor couplings J_{nnn} within the chains.[67] The chain Hamiltonian in a magnetic field *H* is

$$H = J_{nn} \sum_j S_j \cdot S_{j+1} + J_{nnn} \sum_j S_j \cdot S_{j+2} - H \sum_j S_j^z \tag{7}$$

In the case of J_{nnn} being antiferromagnetic ($J_{nnn} > 0$), the chain is frustrated independent of the sign of J_{nn}. If both J_{nn} and J_{nnn} are

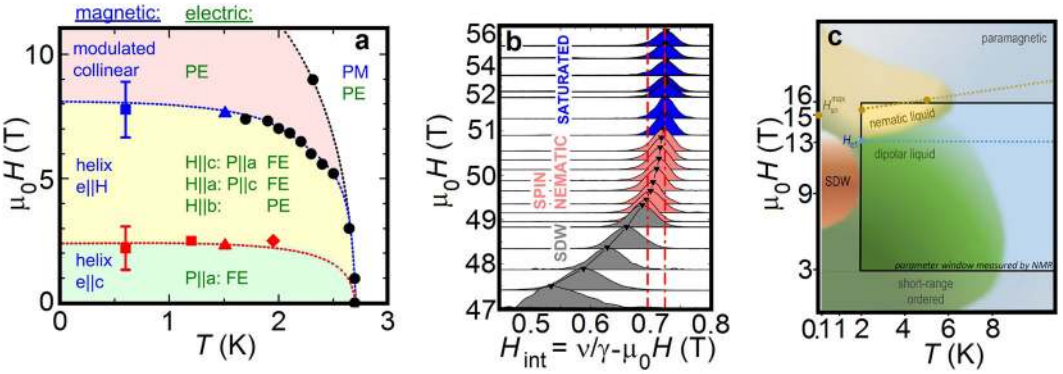

Fig. 5 **a** (H,T) phase diagram of $LiCuVO_4$ (adapted with permission from, ref. [76] copyright American Physical Society 2008). The magnetic and electric states are noted in the figure; **b** ^{51}V NMR spectra in $LiCuVO_4$ for $H||b$ (reproduced with permission from, ref. [78] copyright American Physical Society 2017). The peak of each line is marked by the black triangle. Spin-density wave, spin nematic and saturated field ranges are highlighted by different colors. The dash-dotted lines denote field-dependent H_{int}; **c** (H,T) phase diagram of $LiCuSbO_4$ (adapted with permission from, ref. [79] copyright Springer Nature 2017). The dark red area corresponds to an anomalous spin density wave phase; the dark yellow area depicts a nematic phase. The blue line marks the isosbestic field H_{c1}. The brown circles depict the maximum of the spin-nematic correlation function H_{SN}^{max}

positive, a spin gap opens at $J_{nnn}/J_{nn} = \alpha > \alpha_C = 0.241$.[68] At $\alpha = 0.5$, the Majumdar–Ghosh ground state is represented by a superposition of spin singlets. Tentatively, copper chromate, $CuCrO_4$, is the best realization of this model with $J_{nn} = 54$ K and $J_{nnn} = 27$ K.[69] It should be noted, however, that no spin gap was observed experimentally in the compounds which satisfy the criterion $\alpha > \alpha_C$. If J_{nn} is FM ($J_{nn} < 0$), FM order within the chain is established in the range $-0.25 < \alpha \le 0$. At $\alpha = -0.25$, the system undergoes quantum phase transition to an incommensurate spin helix state.[70] Among recently found species of this type there are several chain cuprates, e.g., $LiCu_2O_2$,[71] Li_2CuZrO_4,[72] $LiCuSbO_4$,[73] etc., which adopt non-collinear magnetic structure. Of special interest is $LiCuVO_4$ which exhibits ferroelectricity at low temperatures and nematicity at high magnetic fields.

In $LiCuVO_4$, the Cu^{2+} ions form isolated spin-1/2 chains along the orthorhombic b axis.[74] The signs of the exchange interactions within the chains differ, i.e., $J_{nn} = -19$ K while $J_{nnn} = 44$ K. The long-range helix order at $T_N = 2.4$ K is triggered by the interchain interaction $J' = -4.6$ K.[75] The ordered moments of Cu^{2+} ions form a spiral spin ground state in the ab plane with incommensurate propagation vector $\mathbf{Q} = (0;0.532;0)$. $LiCuVO_4$ is an improper ferroelectric with the long-range polar order induced at the onset of a spiral spin order. Measurements of magnetic-field-dependent dielectric constant ε and electrical polarization P allow the construction of a magnetoelectric phase diagram (Fig. 5a).[76] At $T < T_N$ and $H < H_1$ ~2.5 T, the normal vector **e** to (**a**,**b**) helix in $LiCuVO_4$ is parallel to the c axis. At a critical field H_1 ~2.5 T, the vector **e** is turned into the direction of the external field. According to the symmetry rule of spiral magnets, ferroelectric order is established with the polarization $\mathbf{P} \propto \mathbf{e} \times \mathbf{Q}$ along the a axis. In the range $H_1 < H < H_2$ ~7.5 T, the normal vector **e** reorients along the external magnetic field and, thus, the electrical polarization depends on the direction of the magnetic field. Finally, for external magnetic fields above H_2, the helical spin structure is destroyed and the system is paraelectric for all field directions.

Above H_2, an incommensurate, collinear spin density wave of bound magnon pairs is stabilized in medium magnetic fields by a FM J_{nn}. In high fields just below the saturation of magnetization, these pairs experience a Bose–Einstein condensation into quantum multipolar states. One of these states expected just below the saturation H_S is a quadrupolar state of magnon pairs called a spin nematic state, analogous to a nematic liquid crystal. In a spin nematic state, an energy gap develops in the transverse spin-excitation spectrum making the energy of the two-magnon bound state lower than the energy of the single-magnon state.[77]

The microscopic experimental evidence for the formation of a homogeneous, field-dependent, longitudinal spin state without transverse dipolar order was obtained in nuclear magnetic resonance (NMR) measurements on $LiCuVO_4$ single crystals up to 56 T for both $\boldsymbol{H}||c$ and $\boldsymbol{H}||b$ orientations.[78] Observed was the field-dependent NMR line position without change of its width with respect to the saturated phase, as predicted for a spin nematic phase. Figure 5b shows the field dependencies of the ^{51}V spectra for $\boldsymbol{H}||b$ taken at $T = 1.3$ K. The internal local field H_{int} generated on ^{51}V by the transferred hyperfine coupling from the neighboring Cu^{2+} moments directly measures the local magnetization $\boldsymbol{M}$, and is thus extracted using $H_{int} = \nu(^{51}V)/^{51}\gamma - \mu_0 H$ where ν is the frequency and γ is the gyromagnetic ratio.

Three different regions can be identified in these NMR spectra. At $H > 50.55$ T (43.55 T for $\boldsymbol{H}||c$), the spectra are field independent and consist of narrow and symmetric lines which is characteristic for a saturated homogeneous magnetic phase. At $H < 48.95$ T (42.41 T for $\boldsymbol{H}||c$) there appears a strong line broadening; both linewidth and line position are field dependent, which is consistent with the previously identified spin density wave state. This phase is characterized by a modulated spin polarization, where the moments are collinear with the external field. In the field ranges 48.95÷50.55 T for $\boldsymbol{H}||b$ (42.41÷43.55 T for $\boldsymbol{H}||c$), the line positions change with H as in the spin density waves phase, but their widths remain unchanged relative to those of the saturated phase. This behavior corresponds to the formation of a homogeneous magnetic state as expected for a spin-nematic state.

In variance with $LiCuVO_4$, its newly synthesized counterpart $LiCuSbO_4$ does not exhibit long-range order down to 0.1 K, signifying the weakness or frustration of interchain exchange interactions. Indications on the presence of a field-induced spin-nematic state were obtained in measurements of temperature dependencies of ^7Li nuclear spin lattice relaxation rate, T_1^{-1}, at various fields.[79] Below threshold field $\mu_0 H_{c1} = 13$ T, T_1^{-1} diverges at lowering temperature pointing to approach of magnetically ordered phase. Surprisingly, above this field T_1^{-1} shows drastic suppression of relaxation rate at lowering temperature evidencing a gap in magnetic excitation spectrum. Excluding well established mechanisms for the spin gap formation, i.e., Zeeman effect at saturation magnetization and Dzyaloshinskii-Moriya interaction, it was concluded that an external magnetic field induces a multicomponent spin liquid in $LiCuSbO_4$. According to phase diagram, shown in Fig. 5c, a collinear incommensurate spin

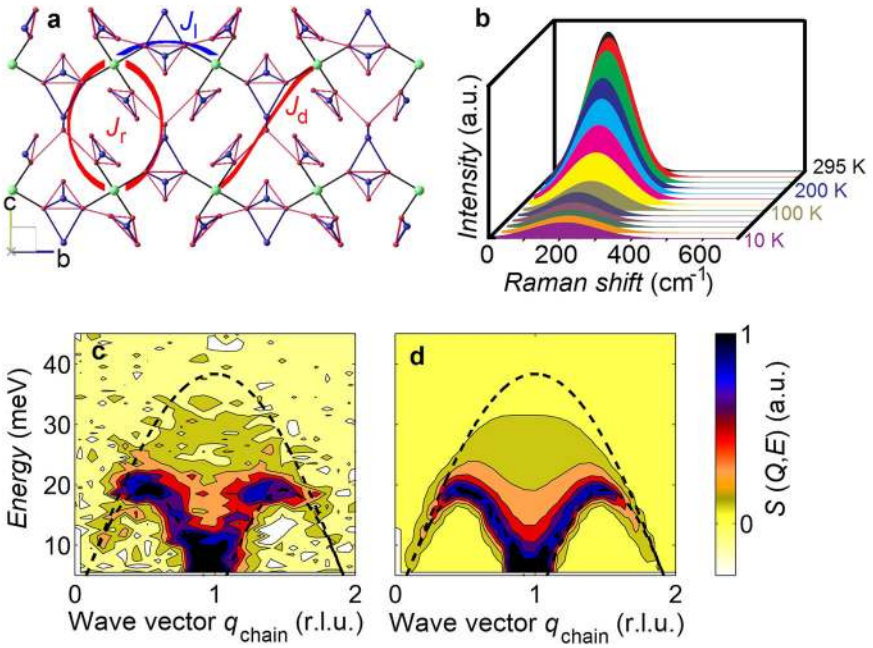

Fig. 6 **a** Nersesyan–Tsvelik pattern in $(NO)Cu(NO_3)_3$ (adapted with permission from, ref. 84 copyright American Physical Society 2010). Arcs denote main exchange interactions between Cu^{2+} ions; **b** magnetic Raman scattering with a finite energy maximum (adapted with permission from, ref. 85 copyright American Physical Society 2012); **c** inelastic neutron scattering data of spinon continuum at 5.5 K (adapted with permission from, ref. 86 copyright American Physical Society 2014); **d** simulation of spinon continuum with $J = 142$ K. The boundary of two-spinon continuum is marked by dashed line (adapted with permission from, ref. 86 copyright American Physical Society 2014)

density wave phase precedes spin-nematic phase, both being gapped. The range of possible multipolar nematic phase was narrowed to 12.5–13 T, recently.[80] Thus, the study of $LiCuSbO_4$ gives further support to the concept that the fragile multipolar phases may survive in low-dimensional magnets due to enhancement of quantum fluctuations in the presence of competing and strongly anisotropic exchange interactions.

LADDERS, NERSESYAN–TSVELIK NETWORK

Isolated magnetic entities consisting of exchange-coupled chains constitute the multitude of spin ladders.[81] The magnetic excitation spectra are gapped for half-integer even leg ladders and gapless for odd leg ladders. In the former case the fractionalized spin -1/2 excitations are confined so that the excitations carry spin 0 and 1. Depending on the ratio of the rung J_r and the leg J_l exchange interactions, various ground states could be formed in these objects. In the case of $J_r \gg J_l$, the even leg ladder can be considered as the collection of weakly interacting dimers. In the opposite case of $J_r \ll J_l$, independent on the number of legs, the pattern is that of weakly interacting gapless chains. In the case of the spin-1 ladder the ground state is gapped for any ratio of J_r and J_l. Of special interest is the Nersesyan–Tsvelik network, which is an extension of the spin-ladder pattern to the layer where both rung J_r and plaquette-diagonal J_d exchange interaction are taken into account.[82]

In the coupled chains model the spin liquid state of the two-dimensional counterpart of one-dimensional spin-1/2 Heisenberg AFM can be realized when the exchange is frustrated in the direction perpendicular to the chains and can be fine-tuned. In the case for which the interchain couplings satisfy the relation $J_r = 2J_d$, the interaction between staggered magnetizations is eliminated completely. Both frustration and spatial anisotropy of exchange interactions are essential ingredients of the Nersesyan–Tsvelik model. The Hamiltonian in this case is

$$H = \sum_{j,n} \left\{ J_l S_{j,n} \cdot S_{j+1,n} + \sum_{\mu=\pm 1} \left[J_r S_{j,n} + J_d \left(S_{j+1,n} + S_{j-1,n} \right) S_{j,n+\mu} \right] \right\} \quad (8)$$

where $S_{j,n}$ are spin-1/2 operators, $J_l, J_r, J_d > 0$ and $J_l \gg J_r, J_d$.

The spatially anisotropic square lattice quantum AFM was analyzed by Starykh and Balents who showed that to realize the Nersesyan–Tsvelik model just the reduction of the coupling of staggered magnetization of different chains is needed, not full elimination.[83] An attempt to verify this model involves the $(NO)Cu(NO_3)_3$. The layered crystal structure of this compound is organized by weakly coupled chains running along the *b* axis, as shown in Fig. 6a.[84] The intrachain exchange interaction, J_l, passes through NO_3^- group which bounds neighboring Cu^{2+} ($S = 1/2$) ions. Within the *bc* plane these ions are coupled by rung exchange interaction, J_r, involving two NO^+ groups and diagonal exchange interaction, J_d, which passes through one NO^+ group. It allows presuming that $J_r = 2J_d$. The interplane exchange interaction along the *a* axis is considered to be small.

The temperature dependencies of both magnetic susceptibility χ and electron spin resonance intensity χ_{ESR} in $(NO)Cu(NO_3)_3$ have been described by the formalism appropriate for isolated half-integer spin chains with $J_l = 170$ K. However, the value of χ at low temperatures was found to be significantly smaller than expected for an isolated spin-1/2 Heisenberg chain. Another probe of the spin liquid state was Raman spectroscopy which evidenced a gapless continuum of magnetic origin (Fig. 6b).[85] The position of the maximum in this continuum defines the major exchange coupling along the chains as $J_l = 150$ K. That same spinon continuum was observed in inelastic neutron scattering (Fig. 6c).[86]

The condition $J_r = 2J_d$ requires a subtle fine tuning of the couplings. The deviation from this ratio may lead to formation of the Neel state at low temperatures. In the band structure calculations, it was admitted that $J_r = 2J_d$ ratio may not be

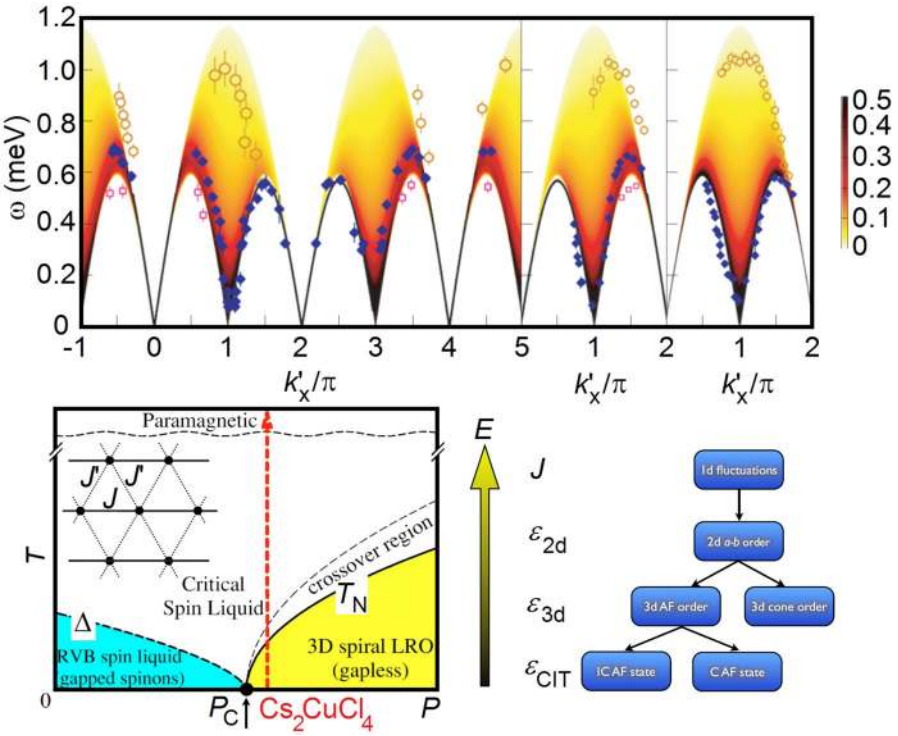

Fig. 7 **a** Dynamical structure factor for dispersion relations at $k_y' = 0$ (left), $k_y' = 2\pi$ (center) and $k_y' = 3\pi$ (right) in Cs_2CuCl_4. (adapted with permission from, ref. 93 copyright Springer Nature 2007, and, ref. 91 copyright American Physical Society 2001). **b** Phase diagram of a quasi-2D frustrated quantum magnet with deconfined spinons near an instability to spiral long-range order driven by a small parameter P in the Hamiltonian (such as the interlayer coupling) (adapted with permission from, ref. 92 copyright American Physical Society 2003). **c** The schematic cascade of energy scales relevant to Cs_2CuCl_4, which is to be considered from largest to smallest (reproduced with permission from, ref. 94 copyright American Physical Society 2010)

fulfilled in $(NO)Cu(NO_3)_3$ because the interaction between NO_3^- units flared out of the plane of Fig. 6c may contribute to J_r but may not contribute to J_d.[87] Indeed, the long-range magnetic order occurs at the highly reduced Neel temperature $T_N = 0.58(5)$K.[86] The large ratio $J_l/T_N \sim 2.5 \times 10^2$ marks the strong suppression of magnetic order. Furthermore, the specific heat C_p and muon spectroscopy (μSR) imply a small ordered moment m while the neutron diffraction gives an upper limit of m ~0.01 μ_B. Evidence that the interchain interactions are competing comes from μSR, which shows that the magnetic order is an incommensurate spin density wave. Since the inelastic neutron scattering reveals commensurate magnetism along the chains, the order must be incommensurate perpendicular to the chains. Hence, the $(NO)Cu(NO_3)_3$ can be considered as a highly one-dimensional chain compound with frustrated interchain interactions. Tentatively, it corresponds to the Nersesyan−Tsvelik model with finite and competing values of J_r and J_d, although the ratio of these interactions and the proximity of the system to the special point $J_r = 2J_d$ is still unknown.

LAYERS, TRIANGULAR, KAGOME AND HONEYCOMB LATTICES

The interest to layered magnets has been triggered by discovery of superconductivity in $La_{2-x}Ba_xCuO_4$ which possesses a square layered magnetic lattice.[88] The issue of quantum ground state in such a lattice belongs to the most complicated ones since the competition of intralayer exchange interactions along with interlayer interactions and anisotropy may significantly influence the long-range ordering processes. The introduction of holes into the copper layers leads to frustration of magnetic interactions and formation of resonating dimer singlets, i.e., mobile Cooper pairs. This allowed Anderson advance a concept of high-T_C superconductivity in cuprates based on idea of resonating valence bond (RVB) state.[89] Such a quantum spin liquid state was suggested initially to describe valence bond interactions in geometrically frustrated 2D system of Mott insulator.[90] To realize the spin liquid state in two dimensions the most obvious candidates are triangular and kagome lattices.

Among triangular 2D spin-1/2 Heisenberg antiferromagnets, Cs_2CuCl_4 is considered to be a closest realization of a quantum spin liquid.[91] Within planes of this compound the copper spins form an anisotropic frustrated network with linear chain coupling J along the b axis and zigzag inter-chain coupling $J' \sim J/3$ along the c axis, as shown in the inset to Fig. 7b. Present are also order of magnitude smaller inter-plane coupling J'' and in-plane Dzyaloshinskii–Moriya term D responsible for incommensurate spiral order at $T_N = 0.62(1)$K.[92] A distinctive feature of Cs_2CuCl_4 revealed by inelastic neutron scattering is the presence of highly dispersive excitation continuum indicative of fractionalization of $S = 1$ spin waves into pairs of deconfined $S = 1/2$ spinons, as shown in Fig. 7a. Below T_N, the sharp excitations appear at low energies, but the dominant continuum at higher energies remains basically unchanged. It was argued by Kohno, Starykh and Balents,[93] that the sharp excitations represent the spinon bound states, i.e., triplons, rather than magnons which are modes of a long-range ordered magnet. The data obtained suggest that Cs_2CuCl_4 could be placed into close proximity to quantum critical point separating fractional resonating-valence-bond (RVB) spin liquid and a magnetically ordered state, as shown in Fig. 7b. In a magnetic field, the phase diagram of Cs_2CuCl_4 has been found to be quite sensitive to smallest interactions.[94] These interactions may induce entirely new phases and are responsible for commensurate-incommensurate transition. A cascade of energy scales pertinent to Cs_2CuCl_4 in a magnetic field oriented along the b axis is represented by Fig. 7c.

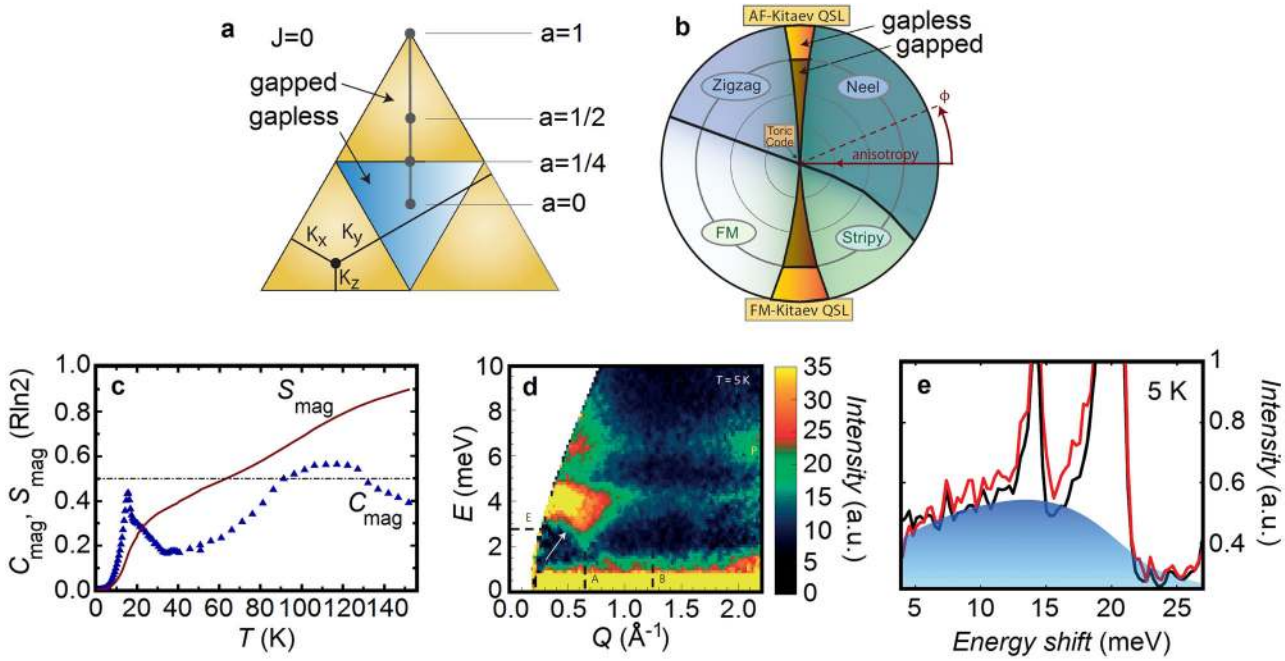

Fig. 8 **a** Kitaev spin liquid with bond anisotropy (reproduced with permission from, ref. 114 copyright American Physical Society 2014); **b** magnetic phases captured by the bond-anisotropic Kitaev−Heisenberg model (reproduced with permission from, ref. 114 copyright American Physical Society 2014); **c** experimental evidence for proximity to the Kitaev quantum spin liquid (QSL): magnetic heat capacity C_{mag} and magnetic entropy S_{mag} in units of Rln2 vs T for Na_2IrO_3. The dash-dotted line corresponds to 1/2Rln2 (reproduced with permission from, ref. 107 copyright American Physical Society 2017); **d** color plot of the data at $T = 5$ K with the magnetic modes ($M1$ and $M2$) detected in inelastic neutron scattering at $E = 4$ and 6 meV. $M1$ shows a minimum near $Q = 0.62$ Å^{-1}, close to the M point of the honeycomb reciprocal lattice. The arrow shows the concavity of the $M1$ mode (adapted with permission from, ref. 108 copyright Springer Nature 2016); **e** structure and polarized Raman response of α-$RuCl_3$ at 5 K. The shaded blue region indicates the continuum contribution (adapted with permission from, ref. 110 copyright American Physical Society 2015)

Quite a few 2D compounds were considered hosting a quantum spin liquid on a geometrically frustrated kagome lattice. Among them, volborthite[95] $Cu_3V_2O_7(OH)_2 \times 2H_2O$, vesignieite[96] $BaCu_3V_2O_8(OH)_2$ and herbertsmithite[97] $ZnCu_3(OH)_6Cl_2$, the last one being a subject of strictest scrutiny. The main copper–copper antiferromagnetic exchange parameter within network of corner-sharing triangles in $ZnCu_3(OH)_6Cl_2$ was estimated as J ~200 K from the slope of $\chi(T)$ curve at $T > 200$ K, but no evidence on long-range order was obtained down to 50 mK.[98] A peculiar feature of herbertsmithite masking its ground properties is an inevitable partial substitution of inter-plane Zn^{2+} by Cu^{2+}. These defects largely define the low temperature magnetic susceptibility χ of $ZnCu_3(OH)_6Cl_2$. To reveal the intrinsic properties of a kagome layer much better is the local probe, i.e., ^{17}O NMR lineshift.[99] Temperature dependence of this property is markedly different from that of a bulk probe. While the $\chi(T)$ dependence resembles the Curie law, ^{17}O NMR lineshift passes through broad maximum at elevated temperatures and becomes temperature-independent at lowest temperatures. The fractional spin excitations in $ZnCu_3(OH)_6Cl_2$ form flat continuum evidenced in neutron scattering measurements. This is a signature of a quantum spin liquid. The key issue in this respect is the presence (or absence) of a spin gap. While it was not established unambiguously, the neutron scattering data set an upper limit for the spin gap value of about 0.1 J, if any.[100] Evidence for a gapped spin-liquid ground state was obtained from the ^{17}O NMR lineshift measurements on herbertsmithite single crystal. It was demonstrated that the intrinsic local susceptibility of kagome lattice tends to zero at $T < 0.03\,J$.[101] These experimental data are crucial to distinguish between various theories on quantum ground state of spin-1/2 Heisenberg AFM on a kagome lattice, including valence-bond solid, gapped and gapless spin liquids.

Among quantum theoretical models of two-dimensional magnets an important role belongs to the Kitaev model where an exact solution for a spin-1/2 honeycomb lattice with anisotropic bond-dependent interactions exists.[102] The ground state in the pure Kitaev model is a quantum spin liquid, either gapped or gapless depending on the exchange interaction parameters (Fig. 8a). Beyond the pure Kitaev limit, four other types of the ground state can be realized in honeycomb lattice dependent on anisotropy and frustration triggered by competition of exchange interactions: FM, Neel's AFM, AFM zigzag and AFM stripe order (Fig. 8b).

The Kitaev model has generated a new trend in the study of quantum spin liquids due to the topological nature of its solution: in contrast to conventionally ordered magnets, which possess bosonic elementary excitations (magnons), in such a state spins $S = 1/2$ are predicted to fractionalize into itinerant Majorana fermions and localized Z_2 fluxes.[103–105] The quantum liquid state preserves all the symmetries of the high-temperature paramagnet even at $T = 0$ K and evade a description by conventional local order parameters, because the fractionalization affects both thermal and dynamic properties of these topological phases. The signatures of the Kitaev spin liquid are (i) two peaks at T_l and T_h in specific heat curves, $C_p(T)$, caused by the fractionalization of spins; (ii) a plateau at 1/2Rln2 in $C_p(T)$ curves in between these peaks; (iii) incoherent spectra of dynamical spin structure factors $S(q,\omega)$, iv) small ratio $T_l/T_h \leq 0.03$.[106]

The most popular candidates for the experimental verification of the Kitaev model have been limited up to now to spin-1/2 systems with 5d and 6d elements, and most importantly A_2IrO_3 (A = Li,Na) and α−$RuCl_3$. Strong spin-orbit coupling was found to play a key role in the formation of anisotropic bond-dependent interactions on the honeycomb lattice in this case. Despite

Table 1. Selected spin gap compounds

Structural units	Compound	Spin gap Δ, K	Comment
Dimers	$SrCu_2(BO_3)_2$	34	Shastry–Sutherland network[13]
	$BaCuSi_2O_6$	52	Bose–Einstein condensation[23]
	$Ba_3Cr_2O_8$	28	Bose–Einstein condensation[115]
	$Sr_3Cr_2O_8$	64	Bose–Einstein condensation[24]
	$Ba_3Mn_2O_8$	19	Bose–Einstein condensation[25]
	$TlCuCl_3$	66	Bose–Einstein condensation[21]
	$Pb_2V_3O_9$	15	Bose–Einstein condensation[22]
	$BaVSi_2O_7$	37	Spin liquid[116]
	$CuAl(AsO_4)O$	350	Spin liquid[117]
Plaquettes	CaV_4O_9	107	Spin liquid[118]
	$NaKV_4O_9{\times}2H_2O$	96	Spin liquid[119]
Half-integer spin chains	$CuGeO_3$	24	Spin-Peierls transition[50]
	NaV_2O_5	114	Charge ordering[56]
	$NaTiSi_2O_6$	620	Orbital ordering[61]
	TiOCl	435	Orbital ordering[120]
	CsV_2O_5	146	Spin liquid[121]
	$(VO)_2P_2O_7$	36, 69	Spin liquid[122]
	$BaCu_2V_2O_8$	230	Spin liquid[39]
Integer spin chains	Y_2BaNiO_5	87÷111	Anisotropic Haldane gap[123]
	$PbNi_2V_2O_8$	14÷25	Anisotropic Haldane gap[48]
	$SrNi_2V_2O_8$	27÷71	Anisotropic Haldane gap[124]
Odd leg ladders	MgV_2O_5	17	Spin liquid[125]
	$SrCu_2O_3$	380	Spin liquid[126]
	CaV_2O_5	600	Spin liquid[125]
Planes	$(CuCl)LaNb_2O_7$	26	Spin liquid[127]
	$Na_3Cu_2SbO_6$	139	Spin liquid[128]
	$Na_2Cu_2TeO_6$	127	Spin liquid[128]
	$(NO)Cu(NO_3)_3$	146	Nersesyan–Tsvelik network[84]

expectations, however, all these compounds do not have a true spin-liquid ground state because they demonstrate long-range AFM order at low temperatures, preceded by a wide maximum on the temperature dependence of the magnetic susceptibility. This cannot be related to Kitaev interactions, originating from the direct exchange between the transition metal ions. At the same time, the properties of these compounds at elevated temperatures reflect the proximity to Kitaev model and remain to be of great interest.

For instance, two peaks in the $C_p(T)$ caused by the fractionalization of spin to two types of Majorana fermions and plateau/shoulder pinned at $1/2R\ln 2$ in $S_{mag}(T)$ have been observed recently for Na_2IrO_3, as shown in Fig. 8c.[107] Fractionalized elementary excitations, reflecting the peculiarity of quantum spin liquid, have been identified in inelastic neutron scattering where they constitute a continuum, sharply distinct from the magnon modes inherent for ordered magnets. Such incoherent spectra were observed in inelastic neutron scattering[108,109] (Fig. 8d) and Raman experiments (Fig. 8e) in α−$RuCl_3$.[110,111]

The BKT paradigm formulated initially for the frustrated square lattice can be extended to triangular, kagome and honeycomb systems also. This concept presumes a phase transition from unbound vortex and antivortex state of two-dimensional magnet to the coupled vortex–antivortex phase at low temperatures. Below critical temperature of this transition, the formation of topological defects (vortex-antivortex pairs) leads to the appearance of additional degree of freedom, i.e., chirality.

CONCLUSION

The versatile phenomena seen in low-D quantum magnets are just mentioned here in an introductory manner. Each of these phenomena deserves a separate review papers, interested readers are respectfully referred to them. The choice of milestones in the field of low-dimensional magnetism is highly debatable. There cannot be unambiguous criteria for importance, timeliness or impact on the scientific community. Several advanced models and concepts of low-dimensional magnetism, for example the BKT transition or the Kitaev model, are still waiting for a rigorous experimental verification. Quite recently, a new member of honeycomb iridates family, Cu_2IrO_3, becomes available. Its *C*2/c structure with bond angles close to 120° fits almost perfectly the Kitaev model. Although Cu_2IrO_3 experiences weak magnetic order at 2.7 K, its high frustration ratio of about 40 and sensitivity of the transition to magnetic field evidences its proximity to quantum spin liquid state.[112] Similarly, a new candidate for the realization of quantum spin liquid state on a kagome lattice has appeared recently. It is kapellasite-type cuprate $YCu_3(OH)_6Cl_3$ where no mixing of Y^{3+} and Cu^{2+} suggests even better realization of perfect kagome than herbertsmithite.[113] Despite high Curie–Weiss temperature of about 100 K this compound exhibit no long-range order down to 2 K. The list of chosen spin-gap compounds is given in Table 1. There are not many, and the gapless spin-liquids are even scarcer. Fortunately, every new compound with an exotic ground state and non-trivial excitations brings new colors to the palette of quantum cooperative phenomena in solids and brings new inspiration to researches concentrated on this fascinating topic.

ACKNOWLEDGEMENTS

The useful comments of Peter Lemmens, Hiroshi Kageyama and John Coulson are gratefully acknowledged. Support of Russian Foundation for Basic Research through grants 17-02-00211, 17-52-45014 and 18-02-00326 is acknowledged. This work has been supported also by the Russian Ministry of Education and Science of the Russian Federation through NUST «MISiS» grant K2-2017-084 and by the Act 211 of the Government of Russia, contracts 02.A03.21.0004 and 02.A03.21.0011.

AUTHOR CONTRIBUTIONS

A.V. conceived the outline of the paper and wrote "Chains, phase transitions, long-range order" and "Ladders, Nersesyan–Tsvelik network". O.V. wrote "Chains, spin liquids" and "Chains, phase transitions, spin gap" sections. E.Z. wrote "Layers, triangular, kagome and honeycomb lattices" section. M.M. wrote "Dimers, Shastry–Sutherland network" and "Dimers, Bose–Einstein condensation" sections. All authors contributed to "Introduction" and "Conclusion" sections.

ADDITIONAL INFORMATION

Competing interests: The authors declare no competing interests.

Publisher's note: Springer Nature remains neutral with regard to jurisdictional claims in published maps and institutional affiliations.

REFERENCES

1. Ising, E. Report on the theory of ferromagnetism. *Z. Phys.* **31**, 253–258 (1925).
2. Heisenberg, W. On the theory of ferromagnetism. *Z. Phys.* **49**, 619–636 (1928).
3. Bethe, H. Metal theory. *Z. Phys.* **71**, 205–226 (1931).
4. Onsager, L. Crystal statistics I. A two-dimensional model with an order-disorder transition. *Phys. Rev.* **65**, 117–149 (1944).
5. Mermin, N. D. & Wagner, H. Absense of ferromagnetism or antiferromagnetism in one- or two-dimensional isotropic Heisenberg models. *Phys. Rev. Lett.* **17**, 1133–1136 (1966).
6. Berezinskii, V. L. Destruction of long-range order in one-dimensional and two-dimensional systems possessing a continuous symmetry group. II. Quantum systems. *Sov. Phys. JETP* **34**, 610–616 (1972).
7. Kosterlitz, J. M. & Thouless, D. J. Long range order and metastability in two dimensional solids and superfluids. *J. Phys. C. Solid State Phys.* **5**, L124–L126 (1972).
8. Kosterlitz, J. M. & Thouless, D. J. Ordering, metastability and phase transitions in two-dimensional systems. *J. Phys. C. Solid State Phys.* **6**, 1181–1203 (1973).
9. Haldane, F. D. M. Continuum dynamics of the 1-D Heisenberg anti-ferromagnet identification with the O(3) non-linear sigma-model. *Phys. Lett. A* **93**, 464–468 (1983).
10. Giamarchi, T., Ruegg, C. & Tchernyshyov, O. *Nat. Phys.* **4**, 198–204 (2008).
11. Shastry, B. S. & Sutherland, B. Exact ground state of quantum-mechanical antiferromagnet. *Phys. B* **108**, 1069–1070 (1981).
12. Miyahara, S. & Ueda, K. Exact dimer ground state of the two dimensional Heisenberg spin system $SrCu_2(BO_3)_2$. *Phys. Rev. Lett.* **82**, 3701–3704 (1999).
13. Kageyama, H. et al. Exact dimer ground state and quantized magnetization plateaus in the two-dimensional spin system $SrCu_2(BO_3)_2$. *Phys. Rev. Lett.* **82**, 3168–3171 (1999).
14. Kageyama, H. et al. Direct evidence for the localized single-triplet excitations and the dispersive multitriplet excitations in $SrCu_2(BO_3)_2$. *Phys. Rev. Lett.* **84**, 5876–5879 (2000).
15. Takigawa, M. et al. Incomplete devil's staircase in the magnetization curve of $SrCu_2(BO_3)_2$. *Phys. Rev. Lett.* **110**, 067210 (2013).
16. Matsuda, Y. H. et al. Magnetization of $SrCu_2(BO_3)_2$ in ultrahigh magnetic fields up to 118 T. *Phys. Rev. Lett.* **111**, 137204 (2013).
17. Corboz, P. & Mila, F. Crystals of bound states in the magnetization plateaus of the Shastry – Sutherland model. *Phys. Rev. Lett.* **112**, 147203 (2014).
18. Koga, A. & Kawakami, N. Quantum phase transitions in the Shastry—Sutherland model for $SrCu_2(BO_3)_2$. *Phys. Rev. Lett.* **84**, 4461–4464 (2000).
19. Zayed, M. E. et al. 4-spin plaquette singlet state in the Shastry–Sutherland compound $SrCu_2(BO_3)_2$. *Nat. Phys.* **13**, 962–966 (2017).
20. Matsubara, T. & Matsuda, H. A lattice model of liquid helium, I. *Prog. Theor. Phys.* **16**, 569–582 (1956).
21. Nikuni, T., Oshikawa, M., Oosawa, A. & Tanaka, H. Bose–Einstein condensation of dilute magnons in $TlCuCl_3$. *Phys. Rev. Lett.* **84**, 5868–5871 (2000).
22. Waki, T. et al. Observation of Bose–Einstein condensation of triplons in quasi 1D spin-gap system $Pb_2V_3O_9$. *J. Phys. Soc. Jpn.* **73**, 3435–3438 (2005).
23. Jaime, M. et al. Magnetic-field-induced condensation of triplons in Han purple pigment $BaCuSi_2O_6$. *Phys. Rev. Lett.* **93**, 087203 (2009).
24. Aczel, A. A. et al. Field-induced Bose–Einstein condensation of triplons up to 8 K in $Sr_3Cr_2O_8$. *Phys. Rev. Lett.* **103**, 207203 (2009).
25. Samulon, E. C. et al. Asymmetric quintuplet condensation in the frustrated S = 1 spin dimer compound $Ba_3Mn_2O_8$. *Phys. Rev. Lett.* **103**, 047202 (2009).
26. Manaka, H. et al. Field-induced magnetic long-range order in the ferromagnetic-antiferromagnetic alternating Heisenberg chain system $(CH_3)_2CHNH_3CuCl_3$ observed by specific heat measurements. *J. Phys. Soc. Jpn.* **67**, 3913–3917 (1998).
27. Zapf, V. S. et al. Bose-Einstein Condensation of S=1 nickel spin degrees of freedom in $NiCl_2$-4SC$(NH_2)_2$. *Phys. Rev. Lett.* **96**, 077204 (2006).
28. Zapf, V., Jaime, M. & Batista, C. D. Bose–Einstein condensation in quantum magnets. *Rev. Mod. Phys.* **86**, 563–614 (2014).
29. Samulon, E. C. et al. Ordered magnetic phases of the frustrated spin-dimer compound $Ba_3Mn_2O_8$. *Phys. Rev. B* **77**, 214441 (2008).
30. Lieb, E., Schultz, T. & Mattis, D. Two soluble models of an antiferromagnetic chain. *Ann. Phys.* **16**, 407–466 (1961).
31. Bonner, J. C. & Fisher, M. E. Linear magnetic chains with anisotropic coupling. *Phys. Rev. A* **135**, 640–658 (1964).
32. Belik, A. A., Azuma, M. & Takano, M. Characterization of quasi-one-dimensional S=1/2 Heisenberg antiferromagnets $Sr_2Cu(PO_4)_2$ and $Ba_2Cu(PO_4)_2$ with magnetic susceptibility, specific heat, and thermal analysis. *J. Solid State Chem.* **177**, 883–888 (2004).
33. Johannes, M. D., Richter, J., Drechsler, S.-L. & Rosner, H. $Sr_2Cu(PO_4)_2$: a real material realization of the one-dimensional nearest neighbor Heisenberg chain. *Phys. Rev. B* **74**, 174435 (2006).
34. Belik, A. A., Uji, S., Terashima, T. & Takayama-Muromachi, E. Long-range magnetic ordering of quasi-one-dimensional S=1/2 Heisenberg antiferromagnet $Sr_2Cu(PO_4)_2$. *J. Solid State Chem.* **178**, 3461–3463 (2005).
35. Bonner, J. C. & Blöte, H. W. J. Excitation spectra of the linear alternating antiferromagnet. *Phys. Rev. B* **25**, 6959–6980 (1982).
36. Johnston, D. C. et al. Thermodynamics of spin S = 1/2 antiferromagnetic uniform and alternating-exchange Heisenberg chains. *Phys. Rev. B* **61**, 9558–9606 (2000).
37. Kokado, S. & Suzuki, N. Dynamical structure factor of S = 1/2 AF–F alternating chains. *J. Phys. Soc. Jpn* **68**, 3091–3094 (1999).
38. Borras-Almenar et al. Alternating chains with ferromagnetic and antiferromagnetic interactions. *Theory Magn. Prop. Inorg. Chem.* **33**, 5171–5175 (1994).
39. He, Z., Kyomen, T. & Itoh, M. $BaCu_2V_2O_8$: Quasi-one-dimensional alternating chain compound with a large spin gap. *Phys. Rev. B* **69**, 220407 (2004).
40. Ghoshray, K. et al. ^{51}V NMR study of the quasi-one-dimensional alternating chain compound $BaCu_2V_2O_8$. *Phys. Rev. B* **71**, 214401 (2005).
41. Koo, H.-J. & Whangbo, M.-H. Importance of the O−M−O Bridges (M=V^{5+}, Mo^{6+}) for the spin-exchange interactions in the magnetic oxides of Cu^{2+} ions bridged by MO_4 tetrahedra: spin-lattice models of $Rb_2Cu_2(MoO_4)_3$, $BaCu_2V_2O_8$, and $KBa_3Ca_4Cu_3V_7O_{28}$. *Inorg. Chem.* **45**, 4440–4447 (2006).
42. Salunke, S. S., Mahajan, A. V. & Dasgupta, I. Magnetic properties and electronic structure of S=1/2 spin gap compound $BaCu_2V_2O_8$. *Phys. Rev. B* **77**, 012410 (2008).
43. Klyushina, E. S. et al. Magnetic excitations in the S = 1/2 antiferromagnetic-ferromagnetic chain compound $BaCu_2V_2O_8$ at zero and finite temperature. *Phys. Rev. B* **93**, 241109 (2016).
44. Haldane, F. D. M. Nonlinear theory of large-spin Heisenberg antiferromagnets: semiclassically quantized solitons of the one-dimensional easy-axis Neel state. *Phys. Rev. Lett.* **50**, 1153–1156 (1983).
45. Botet, R. & Jullien, R. Ground state properties of a spin-1 antiferromagnetic chain. *Phys. Rev. B* **27**, 613–615 (1983).
46. Nightingale, M. P. & Blote, H. W. J. Gap of the linear spin-1 Heisenberg antiferromagnet: a Monte Carlo calculation. *Phys. Rev. B* **33**, 659–661 (1983).
47. Uchiyama, Y. et al. Spin-vacancy-induced long-range order in a new Haldane-gap antiferromagnet. *Phys. Rev. Lett.* **83**, 632–635 (1999).
48. Zheludev, A. et al. Magnetic excitations in coupled Haldane spin chains near the quantum critical point. *Phys. Rev. B* **62**, 8921–8930 (2000).
49. Bray, J. W. et al. Observation of a spin-Peierls transition in a Heisenberg antiferromagnetic linear-chain system. *Phys. Rev. Lett.* **35**, 744–747 (1975).
50. Hase, M., Terasaki, I. & Uchinokura, K. Observation of the spin-Peierls transition in linear Cu^{2+} (spin-1/2) chains in an inorganic compound $CuGeO_3$. *Phys. Rev. Lett.* **70**, 3651–3654 (1993).
51. Bulaevskii, L. N., Buzdin, A. I. & Khomskii, D. I. Spin – Peierls transition in magnetic field. *Solid State Commun.* **27**, 5 (1978).
52. Nishi, M., Fujita, O. & Akimitsu, J. Neutron-scattering study on the spin-Peierls transition in a quasi-one-dimensional magnet $CuGeO_3$. *Phys. Rev. B* **50**, 6508–6510 (1979).
53. Northby, J. A. et al. Field-dependent differential susceptibility studies on tetrathiafulvalene-$AuS_4C_4(CF_3)_4$: Universal aspects of the spin-Peierls phase diagram. *Phys. Rev. B* **25**, 3215–3225 (1982).
54. Hase, M. et al. Magnetic phase diagram of the spin-Peierls cuprate $CuGeO_3$. *Phys. Rev. B* **48**, 9616–9619 (1993).
55. Nojiri, H. et al. Observation of magnetization saturation of $CuGeO_3$ in ultrahigh magnetic fields up to 500 T. *Phys. Rev. B* **55**, 12749–12754 (1995).
56. Isobe, M. & Ueda, Y. Magnetic susceptibility of quasi-one-dimensional compound alpha'-NaV_2O_5 - possible spin-Peierls compound with high critical temperature of 34K. *J. Phys. Soc. Jpn.* **65**, 1178–1181 (1996).
57. Ohama, T., Yasuoka, H., Isobe, M. & Ueda, Y. Mixed valency and charge ordering in alpha'-NaV_2O_5. *Phys. Rev. B* **59**, 3299–3302 (1999).
58. Sawa, H. et al. low-temperature structure of the quarter-filled ladder compound alpha'-NaV_2O_5. *J. Phys. Soc. Jpn.* **71**, 385–388 (2002).
59. Nakao., H. et al. X-ray anomalous scattering study of a charge-ordered state in NaV_2O_5. *Phys. Rev. Lett.* **85**, 4349–4352 (2000).
60. Ohwada, K. et al. "Devil's staircase"-type phase transition in NaV_2O_5 under high pressure. *Phys. Rev. Lett.* **87**, 086402 (2001).
61. Isobe, M., Ninomiya, E., Vasil'ev, A. N. & Ueda, Y. Novel phase transition in spin-1/2 linear chain systems: $NaTiSi_2O_6$ and $LiTiSi_2O_6$. *J. Phys. Soc. Jpn.* **71**, 1423–1426 (2002).
62. van Wezel, J. & van den Brink, J. Orbital-assisted Peierls state in $NaTiSi_2O_6$. *Europhys. Lett.* **75**, 957–963 (2006).
63. Redhammer, G. J., Ohashi, H. & Roth, G. Single-crystal structure refinement of $NaTiSi_2O_6$ clinopyroxene at low temperatures (298<T<100 K). *Acta Cryst. B* **59**, 730–746 (2003).

64. Konstantinovic, M. J. et al. Orbital dimerization in $NaTiSi_2O_6$: an orbital analogue of the spin-Peierls phase transition. *Phys. Rev. B* **69**, 020409 (2004).
65. Silverstein, H. J. et al. Direct measurement of the spin gap in a quasi-one-dimensional clinopyroxene: $NaTiSi_2O_6$. *Phys. Rev. B* **90**, 140402 (2014).
66. Hikihara, T. & Motome, Y. Orbital and spin interplay in spin-gap formation in pyroxene $ATiSi_2O_6$ (A=Na, Li). *Phys. Rev. B* **70**, 214404 (2004).
67. Drechsler, S.-L. et al. Helimagnetism and weak ferromagnetism in edge-shared chain cuprates. *J. Magn. Magn. Mater.* **316**, 306–312 (2007).
68. Lebernegg, S. et al. Frustrated spin chain physics near the Majumdar-Ghosh point in szenicsite $Cu_3(MoO_4)(OH)_4$. *Phys. Rev. B* **95**, 035145 (2017).
69. Law, J. M. et al. Quasi-one-dimensional antiferromagnetisn and multiferroicity in $CuCrO_4$. *Phys. Rev. B* **84**, 014426 (2011).
70. Hikihara, T., Kecke, L., Momoi, T. & Furusaki, A. Vector chiral and multipolar orders in the spin-1/2 frustrated ferromagnetic chain in magnetic field. *Phys. Rev. B* **78**, 144404 (2008).
71. Masuda, T., Zheludev, A., Bush, A., Markina, M. & Vasiliev, A. Competition between helimagnetism and commensurate quantum spin correlations in $LiCu_2O_2$. *Phys. Rev. Lett.* **92**, 177201 (2004).
72. Drechsler, S.-L. et al. Frustrated cuprate route from antiferromagnetic to ferromagnetic spin-1/2 Heisenberg chains: Li_2ZrCuO_4 as a missing link near the quantum critical point. *Phys. Rev. Lett.* **98**, 077202 (2007).
73. Dutton, S. E. et al. Quantum spin liquid in frustrated one-dimensional $LiCuSbO_4$. *Phys. Rev. Lett.* **108**, 187206 (2012).
74. Vasil'ev, A. N. et al. Magnetic and resonant properties of quasi-one-dimensional antiferromagnet $LiCuVO_4$. *Phys. Rev. B* **64**, 024419 (2001).
75. Enderle, M. et al. Quantum helimagnetism of the frustrated spin-1/2 chain $LiCuVO_4$. *Europhys. Lett.* **70**, 237–243 (2005).
76. Schrettle, F. et al. Switching the ferroelectric polarization in the spin S=1/2 chain cuprate $LiCuVO_4$ by external magnetic fields. *Phys. Rev. B* **77**, 144101 (2008).
77. Mourigal, M. et al. Evidence of a bond-nematic phase in $LiCuVO_4$. *Phys. Rev. Lett.* **109**, 127203 (2012).
78. Orlova, A. et al. Nuclear magnetic resonance signature of the spin-nematic phase in $LiCuVO_4$ at high magnetic fields. *Phys. Rev. Lett.* **118**, 247201 (2017).
79. Grafe, H.-J. et al. Signatures of a magnetic field-induced unconventional nematic liquid in the frustrated and anisotropic spin-chain cuprate $LiCuSbO_4$. *Sci. Rep.* **7**, 6720 (2017).
80. Bosiocic, M. et al. Possible quadrupolar nematic phase in the frustrated spin chain $LiCuSbO_4$: An NMR investigation. *Phys. Rev. B* **96**, 224424 (2017).
81. Dagotto, E. & Rice, T. M. Surprises on the way from one- to two-dimensional magnets: The ladder materials. *Science* **271**, 618–623 (1996).
82. Nersesyan, A. A. & Tsvelik, A. M. Spinons in more than one dimension: Resonance valence bond state stabilized by frustration. *Phys. Rev. B* **67**, 024402 (2003).
83. Starykh, O. A. & Balents, L. Dimerized phase and transitions in a spatially anisotropic square lattice antiferromagnet. *Phys. Rev. Lett.* **93**, 127202 (2004).
84. Volkova, O. et al. Realization of the Nersesyan-Tsvelik model in $(NO)Cu[(NO_3)_3]$. *Phys. Rev. B* **82**, 054413 (2010).
85. Gnezdilov, V. et al. Dynamical lattice instability versus spin liquid state in a frustrated spin chain system. *Phys. Rev. B* **85**, 214403 (2012).
86. Balz, C. et al. Quantum spin chain as a potential realization of the Nersesyan-Tsvelik model. *Phys. Rev. B* **90**, 060409 (2014).
87. Janson, O., Tsirlin, A. A. & Rosner, H. Antiferromagnetic spin-1/2 chains in $(NO)Cu(NO_3)_3$: a microscopic study. *Phys. Rev. B* **82**, 184410 (2010).
88. Bednorz, J. G. & Muller, K. A. Possible high T_C superconductivity in the Ba-La-Cu-O system. *Z. Phys. B* **64**, 189–193 (1986).
89. Anderson, P. W. The resonating valence bond state in La_2CuO_4 and superconductivity. *Science* **235**, 1196–1198 (1987).
90. Anderson, P. W. Resonating valence bond—new kind of insulator. *Mater. Res. Bull.* **8**, 153–160 (1973).
91. Coldea, R., Tennant, D. A., Tsvelik, A. M. & Tylczynski, Z. Experimental realization of a 2D fractional quantum spin liquid. *Phys. Rev. Lett.* **86**, 1335–1338 (2001).
92. Coldea, R., Tennant, D. A. & Tylczynski, Z. Extended scattering continua characteristic of spin fractionalization in the two-dimensional frustrated quantum magnet Cs_2CuCl_4 observed by neutron scattering. *Phys. Rev. B* **68**, 134424 (2003).
93. Kohno, M., Starykh, O. A. & Balents, L. Spinons and triplons in spatially anisotropic frustrated antiferromagnets. *Nat. Phys.* **3**, 790–795 (2007).
94. Starykh, O. A., Katsura, H. & Balents, L. Extreme sensitivity of a frustrated quantum magnet: Cs2CuCl4. *Phys. Rev. B* **82**, 014421 (2010).
95. Hiroi, Z. et al. Spin-1/2 kagome-like lattice in volborthite $Cu_3V_2O_7(OH)_2{\times}_2H_2O$. *J. Phys. Soc. Jpn.* **70**, 3377–3384 (2001).
96. Okamoto, Y., Yoshida, H. & Hiroi, Z. Vesignieite $BaCu_3V_2O_8(OH)_2$ as a candidate spin-1/2 kagome antiferromagnet. *J. Phys. Soc. Jpn.* **78**, 033701 (2009).
97. Shores, M. P., Nytko, E. A., Bartlett, B. M. & Nocera, D. G. A structurally perfect S=1/2 kagome antiferromagnet. *J. Am. Chem. Soc.* **127**, 13462 (2005).
98. Helton, J. S. et al. Spin dynamics of the spin-1/2 kagome lattice antiferromagnet $ZnCu_3(OH)_6Cl_2$. *Phys. Rev. Lett.* **98**, 107204 (2007).
99. Olariu, A. et al. ^{17}O NMR study of the intrinsic magnetic susceptibility and spin dynamics of the quantum kagome antiferromagnet $ZnCu_3(OH)_6Cl_2$. *Phys. Rev. Lett.* **100**, 087202 (2008).
100. Han, T. H. et al. Fractionalized excitations in the spin-liquid state of a kagome-lattice antiferromagnet. *Nature* **492**, 406–410 (2012).
101. Fu, M. X., Imai, T., Han, T. H. & Lee, Y. S. Evidence for a gapped spin-liquid ground state in a kagome Heisenberg antiferromagnet. *Science* **350**, 655 (2015).
102. Kitaev, A. Anyons in an exactly solved model and beyond. *Ann. Phys.* **321**, 2–111 (2006).
103. Lacroix, C., Mendels, P. & Mila, F. *Introduction to Frustrated Magnetism, Springer Series in Solid-State Sciences* (Springer-Verlag, Berlin Heidelberg, 2011).
104. Nasu, J., Udagawa, M. & Motome, Y. Vaporization of Kitaev spin liquids. *Phys. Rev. Lett.* **113**, 197205 (2014).
105. Nasu, J., Udagawa, M. & Motome, Y. Thermal fractionalization of quantum spins in a Kitaev model: Temperature-linear specific heat and coherent transport of Majorana fermions. *Phys. Rev. B* **92**, 115122 (2015).
106. Yamaji, Y. et al. Clues and criteria for designing a Kitaev spin liquid revealed by thermal and spin excitations of the honeycomb iridate Na_2IrO_3. *Phys. Rev. B* **93**, 174425 (2016).
107. Mehlawat, K., Thamizhavel, A. & Singh, Y. Heat capacity evidence for proximity to the Kitaev quantum spin liquid in A_2IrO_3 (A=Na, Li). *Phys. Rev. B* **95**, 144406 (2017).
108. Banerjee, A. et al. Proximate Kitaev quantum spin liquid behavior in a honeycomb magnet. *Nat. Mater.* **15**, 733 (2016).
109. Banerjee, A. et al. Neutron scattering in the proximate quantum spin liquid α-$RuCl_3$. *Science* **356**, 1055 (2017).
110. Sandilands, L. J. et al. Scattering continuum and possible fractionalized excitations in α−$RuCl_3$. *Phys. Rev. Lett.* **114**, 147201 (2015).
111. Glamazda, A. et al. Relation between Kitaev magnetism and structure in α-$RuCl_3$. *Phys. Rev. B* **95**, 174429 (2017).
112. Abramchuk, M. et al. Cu_2IrO_3: a new magnetically frustrated honeycomb iridate. *J. Am. Chem. Soc.* **139**, 15371–15376 (2017).
113. Sun, W., Huang, Y.-X., Nokhrin, S., Pan, Y. & Mi, J.-X. Perfect kagome lattices in $YCu_3(OH)_6Cl_3$: a new candidate for the quantum spin liquid state. *J. Mater. Chem. C.* **4**, 8772–8777 (2016).
114. Kimchi, I., Analytis, J. G. & Vishwanath, A. Three-dimensional quantum spin liquids in models of harmonic-honeycomb iridates and phase diagram in an infinite-D approximation. *Phys. Rev. B* **90**, 205126 (2014).
115. Aczel, A. A. et al. Bose-Einstein condensation of triplons in $Ba_3Cr_2O_8$. *Phys. Rev. B* **79**, 100409 (2009).
116. Vasiliev, A. et al. Barium vanadium silicate $BaVSi_2O_7$: A t(2g) counterpart of of the Han purple compound. *Phys. Rev. B* **87**, 134412 (2013).
117. Vasiliev, A. N. et al. Valence-bond solid as the quantum ground state in honeycomb layered urusovite $CuAl(AsO_4)O$. *Phys. Rev. B* **91**, 144406 (2015).
118. Taniguchi, S. et al. Spin gap behavior of S=1/2 quasi-2-dimensional system CaV_4O_9. *J. Phys. Soc. Jpn.* **64**, 2758–2761 (1995).
119. Cui, M. et al. $NaKV_4O_9{\times}_2H_2O$: a new 2D magnetic compound with a 1/5-depleted square lattice. *Dalton Trans.* **45**, 5234–5239 (2016).
120. Kataev, V. et al. Orbital order in the low-dimensional quantum spin system TiOCl probed by ESR. *Phys. Rev. B* **68**, 140405 (2003).
121. Isobe, M. & Ueda, Y. Magnetic susceptibilities of AV_2O_5 (A=Li and Cs) with square pyramidal V(IV)O_5. *J. Phys. Soc. Jpn.* **65**, 3142–3145 (1996).
122. Johnston, D. C., Johnson, J. W., Goshorn, D. P. & Jacobson, A. J. Magnetic-susceptibility of $(VO)_2P_2O_7$ - a one-dimensional spin-1/2 Heisenberg-antiferromagnet with a ladder spin configuration and a singlet ground-state. *Phys. Rev. B* **35**, 219–222 (1987).
123. Darriet, J. & Regnault, L. P. The compound Y_2BaNiO_5—a new example of a Haldane-gap in a S=1 magnetic chain. *Sol. St. Comm.* **86**, 409–412 (1993).
124. Bera, A. K. et al. Field-induced magnetic ordering and single-ion anisotropy in the quasi-one-dimensional Haldane chain compound $SrNi_2V_2O_8$: a single-crystal investigation. *Phys. Rev. B* **87**, 224423 (2013).
125. Ueda, Y. Vanadate family as spin-gap systems. *Chem. Mater.* **10**, 2653–2664 (1998).
126. Azuma, M., Hiroi, Z., Takano, M., Ishida, K. & Kitaoka, Y. Observation of a spin gap in $SrCu_2O_3$ comprising spin-1/2 quasi-1D 2-leg ladders. *Phys. Rev. Lett.* **73**, 3463–3466 (1994).
127. Kageyama, H. et al. Spin-singlet ground state in two-dimensional S=1/2 frustrated square lattice: $(CuCl)LaNb_2O_7$. *J. Phys. Soc. Jpn.* **74**, 1702–1705 (2005).
128. Miura, Y., Hirai, R., Kobayashi, Y. & Sato, M. Spin gap behavior of $Na_3Cu_2SbO_6$ with distorted honeycomb structure. *J. Phys. Soc. Jpn.* **75**, 084707 (2006).